Defense Technical Information Center Compilation Part Notice

ADP012176

TITLE: Study of NiFe/SiO2 Nanocomposites

DISTRIBUTION: Approved for public release, distribution unlimited

This paper is part of the following report:

TITLE: Nanophase and Nanocomposite Materials IV held in Boston, Massachusetts on November 26-29, 2001

To order the complete compilation report, use: ADA401575

The following component part numbers comprise the compilation report:
ADP012174 thru ADP012259

Mat. Res. Soc. Symp. Proc. Vol. 703 © 2002 Materials Research Society V1.6

Study of NiFe/SiO_2 Nanocomposites

S. Hui[1], Y.D. Zhang[1], T. D. Xiao[1], Mingzhong Wu[2], Shihui Ge[2], W. A. Hines[2], J. I. Budnick[2], M. J. Yacaman[3], and H. E. Troiani[4]
[1]Inframat Corporation, 74 Batterson Park Road, Farmington, CT 06032
[2]Physics Department and IMS, University of Connecticut, Storrs, CT 06269
[3]Department of Chemical Engineering, University of Texas, Austin, TX 78712
[4]CNM and Texas Materials Institute, University of Texas, Austin, TX 78712

ABSTRACT

$(Ni_{75}Fe_{25})_v/(SiO_2)_{1-v}$ nanocomposites with v =0.5, 0.7, and 1.0, where 75 denotes the atomic percent of Ni in the Ni-Fe alloy phase and v denotes the volume fraction of the magnetic constituent in the composite, were synthesized using a wet chemical approach. The x-ray diffraction and TEM experiments show that the synthetic NiFe/SiO_2 is a two-phase composite system in that an amorphous insulating SiO2 layer coats each Ni-Fe particle. The Ni-Fe particle is in a fcc Ni-Fe alloy state. Its size can be controlled over a rather large range between 5 nm to 70 nm by adjusting the reaction parameters. Particular attention was paid to reduce the chemical reaction temperature so as to insure the smallness of the particle size. Meanwhile, measurements of the saturation magnetization indicated that the higher the heat treatment temperature, the more complete the chemical reaction to form the Ni-Fe alloys from precursor materials.

INTRODUCTION

Magnetic nanocrystalline solids offer attractive properties for various applications such as the active component of ferrofluids [1], recording tapes [2], biomedical materials [3], separation techniques [4], as well as permanent magnets and soft magnetic materials [5-6]. Furthermore, nanocompositing opened new opportunities to develop novel magnetic materials [7]. Such materials provide great possibilities for the atomic engineering of materials with specific magnetic properties. Thin film nanocomposites with significantly improved high frequency properties have been developed based on the exchange coupling mechanism [8-9]. By coating magnetic nanoparticles with a second insulating phase, the following improvements could be achieved. Since the distribution of the two phases is homogenous on a nanometer scale, the aggregation of magnetic nanoparticles themselves is greatly limited. In this case, the magnetic materials can retain the nature of the nanocrystals. Therefore, the interaction of the magnetic particles could be adjusted and studied because the magnetic cores are kept at a well-defined distance. Coating the metallic magnetic nanoparticles prevents oxidation since the particles are extremely active and pyrophoric at ambient conditions. Coating with an insulating phase can improve the electrical resistivity of the magnetic materials. This maintains low eddy current losses for soft magnetic materials in high frequency applications. Coating also hinders the diffusion or the grain growth of metallic particles during the formation or sintering of the nanoparticles.

A wide variety of routes have been employed to synthesize magnetic nanocomposites, including sol-gel [10], sputtering [7], electrodeposition [11], high energy ball milling [12], microemulsion and reverse micelle techniques [13]. In order to dramatically increase the electric resistivity of metallic magnetic alloys while retaining their excellent soft magnetic properties (high saturation magnetization, high permeability, high Curie temperature, etc.),

$(Ni_{75}Fe_{25})_v/(SiO_2)_{1-v}$ nanocomposites were synthesized using a wet chemical approach. The magnetic properties of the nanoparticles were investigated for samples treated at different temperatures.

EXPERIMENTAL

Nickel nitrate, iron nitrate, and tetraethoxysilane (TEOS) were used as received from Alfa Aesar. n-Ni-Fe/SiO2 nanocomposites were synthesized using a wet chemical solution technique, followed by oxidation and reduction under a controlled atmosphere at elevated temperatures. Starting materials were mixed in an organic solvent. The solvent is then removed by evaporation at elevated temperature. A further drying process is performed in an oven to obtain porous agglomerates. The agglomerates were then heated in an oxidizing atmosphere for a period of time. An this stage, impurity elements such as carbon, hydrogen, and nitrogen from the starting materials were burned out and the remaining materials precomposite of were nickel oxide, iron oxides, and silica. The precomposite powder was reduced at different temperatures in the range of 400-900 °C to form n-Ni-Fe/SiO_2 composites.

Thermogravimetric analysis (TGA) was conducted to determine the starting and finishing temperature for oxidation. Characterization of the crystal structure and particle size of the synthetic powder was carried out using x-ray diffraction (XRD) and high-resolution transmission electron microscopy (HRTEM). High-resolution transmission electron micrographs were obtained with a JEOL 4000 EX electron microscope. HRTEM specimens were prepared by dispersing the powders in methanol. Drops of this solution were then deposited on a carbon-grid and observed in the microscope. Bright field images, electron diffraction, and lattice images were carried out. The static magnetic properties of the synthetic powder were studied by using Quantum Design SQUID magnetometer at temperatures of 10 K and 300 K. Before the measurements, the samples were weighted accurately and then wrapped carefully in an adhesive tape.

RESULTS AND DISCUSSION

In Figure 1 a typical TGA scan for the composite materials is presented. It can be seen in Figure1 that the unwanted organic start to burn-off at ~ 300 ^{0}C. However, a rather long time may be required to complete the oxidation and "clean" the precursor at this temperature. It appears that a higher temperature (*e.g.,* 500 °C) is necessary to complete the oxidation reactions.

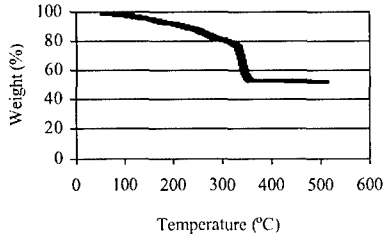

Figure 1. Weight change vs. temperature for precomposite powder of Ni-Fe/SiO_2 in oxygen.

Figure 2 shows the XRD patterns for the $(Ni_{75}Fe_{25})_{0.7}/(SiO_2)_{0.3}$ samples that were obtained by reducing the precursor in H_2 for 3 hours at various temperatures. For a comparison, the figure also includes the XRD pattern of a bulk-size Ni-Fe alloy sample. The results indicate that all of the synthetic $(Ni_{75}Fe_{25})_{0.7}/(SiO_2)_{0.3}$ samples have the face-centered cubic (fcc) structure. As shown in Figure 2, the linewidth of the diffraction peaks for the $(Ni_{75}Fe_{25})_{0.7}/(SiO_2)_{0.3}$ samples were significantly broader than that for the bulk Ni-Fe alloy sample, and highly dependent on the reduction temperature.

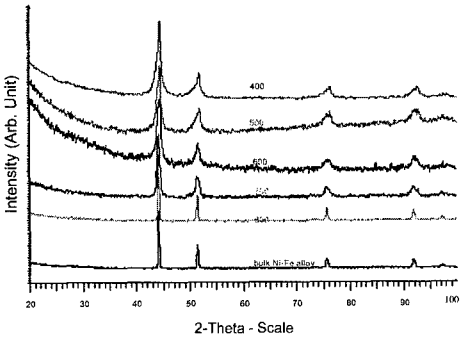

Figure 2. XRD pattern for bulk Ni-Fe alloy and n-$(Ni_{75}Fe_{25})_{0.7}/(SiO_2)_{0.3}$ samples prepared at different reduction temperatures (in degree C).

The particle size for nanostructured materials calculated from the Scherrer equation. Figure 3 shows the particle size of the synthetic $(Ni_{75}Fe_{25})_{0.7}/(SiO_2)_{0.3}$ as a function of the hydrogen reduction temperature. It reveals that when the reduction temperature is 700 °C or below, the particle size remains small (< 20 nm) with little change with reduction temperature. However, the size increases significantly with H_2 reduction temperatures beyond 700 °C.

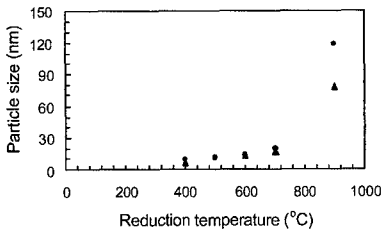

Figure 3. Variation of Ni-Fe particle size with reduction temperature in hydrogen: circles, $(Ni_{75}Fe_{25})_{0.7}/(SiO_2)_{0.3}$; triangles, $(Ni_{75}Fe_{25})_{0.5}/(SiO_2)_{0.5}$.

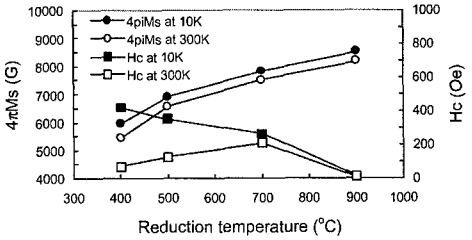

Figure 4. Magnetization and coercivity as a function of H_2 reduction temperature for n-$(Ni_{75}Fe_{25})_{0.7}/(SiO_2)_{0.3}$.

The static magnetic properties of n-$(Ni_{75}Fe_{25})_{0.7}/(SiO_2)_{0.3}$ are summarized in Figure 4 which shows the saturation magnetization and coercivity as a function of the H_2 reduction temperature for $(Ni_{75}Fe_{25})_{0.7}/(SiO_2)_{0.3}$ measured at 10 K and 300 K. The saturation magnetization of the bulk $Ni_{75}Fe_{25}$ alloy is 12000 G, which translates to the saturation magnetization of 8000 G for $(Ni_{75}Fe_{25})_{0.7}/(SiO_2)_{0.3}$ nanocomposite presuming the electronic as well as magnetic structure for the Ni-Fe nanoparticle is essentially the same as those for the bulk Ni-Fe alloy. It can be seen from Figure 4 that for the powder reduced at 900 °C, the saturation magnetization is actually 8600 G. This is due to the composition deviation in that the actual volume fraction of the Ni-Fe magnetic phase may be slightly greater than 0.7. By reducing at 700 °C, a saturation of 8000 G is obtained, which is 93% of the saturation magnetization. This indicates that the reduction temperature can be set to 700 °C at which the reduction process is essentially completed while the Ni-Fe particle size remains less than 20 nm. From Figure 4, it also can be seen that at low temperature the coercivity decreases with increasing reduction temperature, while at room temperature the coercivity increases as the reduction temperature increases from 400 °C to 700 °C. This is probably because some Ni-Fe particles in the nanocomposite reduced at 400 °C and 500 °C have small size due to lower reduction temperature and exhibit superparamagnetic behavior at room temperature.

Figure 5 shows the XRD diffraction patterns for the n-$(Ni_{75}Fe_{25})_{0.5}/(SiO_2)_{0.5}$ powders, which are the same as shown in Figure 2. The particle size dependence on the reduction temperature for n-$(Ni_{75}Fe_{25})_{0.5}/(SiO_2)_{0.5}$ is shown in Figure 3. It is clear that the thicker the SiO_2 coating, the smaller the Ni-Fe particle size obtained in the same reduction process.

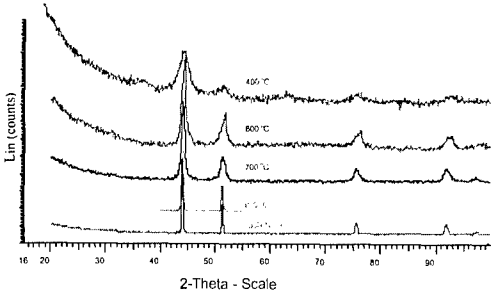

Figure 5. XRD pattern for n-$(Ni_{75}Fe_{25})_{0.5}/(SiO_2)_{0.5}$ and bulk Ni-Fe alloy.

In Figure 6 a typical TEM image is presented which shows the morphology for n-$(Ni_{75}Fe_{25})_{0.5}/(SiO_2)_{0.5}$ sample which was heat-treated in hydrogen at 700 °C. This image shows that all of the particles are embedded in an amorphous media different from the amorphous carbon of the support grid. The image in Figure 7 shows a typical particle size distribution for a portion of the sample. The width of the distribution is approximately 15 nm and it shows a peak centered around 15.5 nm, which is consistent with the size calculated from XRD. The particle range is between 5 and 30 nm, which is a relative large distribution in size. For this histogram, 31 particles were counted and analyzed. The typical length in the figure is an average between the maximum and minimum lateral dimensions measured from the TEM image.

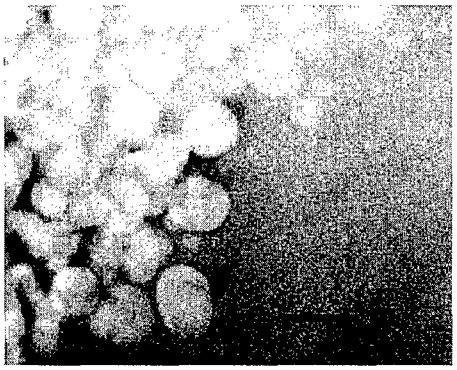

Figure 6. TEM image for the n-$(Ni_{75}Fe_{25})_{0.5}/(SiO_2)_{0.5}$ sample heat-treated in hydrogen at 700 °C. The bar in the figure corresponds to 100 nm.

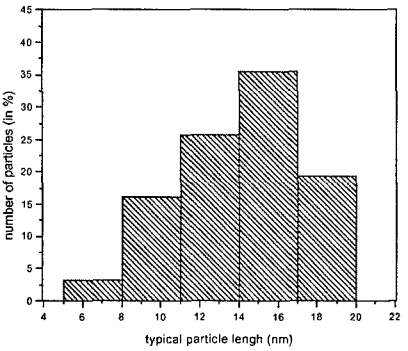

Figure 7. Particle size distribution from TEM study for n-$(Ni_{75}Fe_{25})_{0.5}/(SiO_2)_{0.5}$.

Figure 8 shows the variation of the saturation magnetization and coercivity as a function of reduction temperature in hydrogen. By reducing at 700 °C, a saturation magnetization of 5303 G was obtained. This corresponds to an 84% completion of the chemical reaction. It also can be seen from Figure 8 that, at both 10 K and 300 K, the coercivity decreases when the reduction temperature increases from 600 °C to 900 °C. However, for the nanocomposite reduced at 400 °C, the coercivities measured at 10 K and 300 K are quite different from each other. This may result from the superparamagnetic behavior of small size particles due to the low reduction temperature.

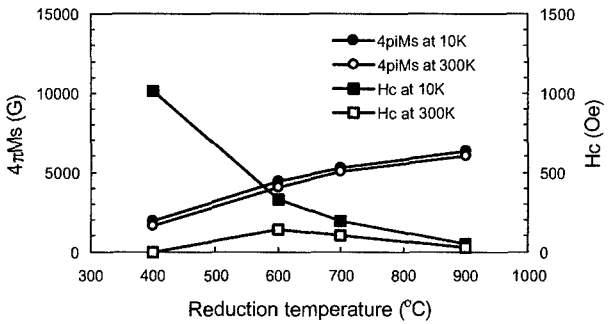

Figure 8. Magnetization and coercivity as a function of reduction temperature in hydrogen for n-$(Ni_{75}Fe_{25})_{0.5}/(SiO_2)_{0.5}$

An interesting result was observed on the $Ni_{75}Fe_{25}$ nanoparticle without a SiO_2 coating. The powder was synthesized using the same chemical route without adding tetraethoxysilane in the starting raw materials. While the powder reduced at 700 °C possesses essentially bulk size (micrometer size), that reduced at 400 °C possesses a mean particle size of only 18.5 nm. For $Ni_{75}Fe_{25}$ powder samples obtained by H_2 reduction at 400 °C and 700 °C respectively, the saturation magnetization for the two samples are the same, indicating that the chemical reaction can be completed at temperatures as low as 400 °C without the existence of SiO_2.

CONCLUSIONS

$(Ni_{75}Fe_{25})_v/(SiO_2)_{1-v}$ (v = 0.5, 0.7) nanocomposites and nanostructured $Ni_{75}Fe_{25}$ alloys have been successfully synthesized using a wet chemical approach. The XRD and TEM studies show that the synthetic Ni-Fe/SiO_2 is a two-phase composite system in that the Ni-Fe particles are embedded in a common amorphous insulating SiO_2 matrix. The Ni-Fe particle is in a fcc Ni-Fe alloy state. Its size can be controlled in a rather large range between 5 nm to 70 nm by adjusting the reaction parameters. Measurements of saturation magnetization indicate that the higher the heat treatment temperature, the more complete the chemical reaction to form the Ni-Fe alloys from the precursor materials.

ACKNOWLEDGMENTS

The work is supported by NASA Contract No. NAS3-01013.

REFERENCES

1. A.P. Philipse, P.B. van Bruggen, and C. Pathmamanoharan, Langmuir **10**, 92-99 (1994).
2. K.O. Grady and H. Laidler, J. Magn. Magn. Mater. **200**, 616-633 (1999).
3. Q. Liu, Z. Xu, J.A. Finch, and R. Egerton, Chem. Mater. **10**, 3936-940 (1998).
4. L. Nixon, C.A. Koval, R.D. Noble, and G.S. Slaff, Chem. Mater. **4**, 117-121 (1992).
5. G.C. Hadjipanayis, WTEC Workshop Rep. R&D Status Trends Nanopart., Nanostruct. Mater., Nanodevices U. S., Proc., Meeting Date 1997 (International Technology Research Institute, Baltimore, Md, 1998), p. 107-112.
6. H. Fukunaga, Nippon Oyo Jiki Gakkaishi **19**(4), 791-6 (1995).
7. G.C. Hadjipanayis and G.A. Prinz, Science and Technology of Nanostructures Magnetic Materials (Plunum Press, New York, 1991).p.477.
8. Y. Hayakawa, A. Makino, H. Fujimori, and A. Inoue, J. Appl. Phys. **81**, 3747 (1997).
9. H. Fujimori, Sripta Met. Mat. **33**, 1625 (1995).
10. (a) G.M. Chow and K.E. Gonsalves, Novel Tech. Synth. Process. Adv. Mater., Proc. Symp. (1994), 155-63. Editor(s): J. Singh and S.M. Copley, Minerals, Metals & Materials Society, Warrendale, Pa.; (b) R. Monaci, A. Musinu, G. Piccaluga, G. Pinna, Mater. Sci. Forum (1995), 195 (Nanophase Materials), 1-6; (c) D. Niznansky, N. Viart, and J.L. Rehspringer, J. Sol-Gel Sci. Tech. **8**, 615-618 (1997).
11. R.D. Shull and L.H. Bennett, Nanostruct. Mater. **1**, 83-88 (1992).
12. (a) A.K. Giri, C. de Julian, J.M. Gonzalez, J. Appl. Phys. **76**(10, Pt. 2), 6573-5 (1994); (b) M. Pardavi-Horvath and L. Takacs, IEEE Trans. Magn. **28**, 3186-3188 (1992).
13. (a) S. Chang, L. Liu, and S.A. Asher, J. Am. Chem. Soc. **116**, 6739 (1994); (b) **116**, 6745 (1994).